Temperature Dependence of Oxygen Reduction Activity at Pt−Fe, Pt−Co, and Pt−Ni Alloy Electrodes

Noriaki Wakabayashi,[†] Masayuki Takeichi,[‡] Hiroyuki Uchida,[‡] and Masahiro Watanabe*,[†]

Clean Energy Research Center, University of Yamanashi, Takeda 4, Kofu 400-8510, Japan, and Interdisciplinary Graduate School of Medicine and Engineering, University of Yamanashi, Takeda 4, Kofu 400-8511, Japan

Received: August 23, 2004; In Final Form: January 27, 2005

Oxygen reduction reaction (ORR) activity and H_2O_2 formation at $Pt_{54}Fe_{46}$, $Pt_{68}Co_{32}$, and $Pt_{63}Ni_{37}$ electrodes in 0.1 M $HClO_4$ solution at 20 to 90 °C were investigated by using a channel flow double electrode method. In the temperature range of 20−50 °C, the apparent rate constants k_{app} for ORR at these electrodes were found to be 2.4−4.0 times larger than that at a pure Pt electrode, whereas their apparent activation energies of 41 kJ mol^{-1} at −0.525 V vs $E°$ (0.760 V vs RHE at 30 °C) were comparable to that at the Pt electrode. H_2O_2 yield was ca. 1.0% at $Pt_{54}Fe_{46}$ and ca. 0.16% at $Pt_{68}Co_{32}$ and $Pt_{63}Ni_{37}$ between 0.3 and 1.0 V vs RHE. The k_{app} values at the alloy electrodes decreased with elevating temperature above 60 °C, and settled to almost the same values at the Pt electrode. The H_2O_2 production was not detected at the alloy electrodes once heated at the high temperature in the solution, probably due to the thickening of the Pt skin-layer by a considerable dissolution of nonprecious metal components (Fe, Co, Ni) from the alloys.

1. Introduction

Development of the highly active cathode catalysts for oxygen reduction reaction (ORR) is one of the most important subjects to achieve a high efficiency at polymer electrolyte fuel cells (PEFCs), which have attracted great interest as a primary power source. Enhanced ORR activities of Pt alloyed with nonprecious metals such as Fe,[1−4] Co,[1,4−8] Ni,[1,3−11] Mn,[4] Cr,[5−7,12,13] and V[14] have been reported in acidic electrolyte solutions. Besides a precise evaluation of a kinetically controlled ORR activity at the electrode, it is important to quantify a reaction byproduct, H_2O_2, which may deteriorate the polymer electrolyte membranes or gaskets. For these two aims, a rotating ring-disk electrode (RRDE) has been employed to examine the ORR at bulk or film alloys[1−3,8−10,12] around room temperature. However, PEFCs should be operated at high temperature (≥80 °C) to improve the ORR activity. There is little systematic research on the temperature dependencies of the ORR activities with/without the simultaneous detection of H_2O_2, because it is difficult to correct the change in the oxygen concentration in the electrolyte solution in the RRDE cell opened to the atmosphere at elevated temperature.

Recently, we have demonstrated that an apparent rate constant k_{app} and apparent activation energy ϵ_a for the ORR at a Pt electrode can be precisely evaluated at 20 to 90 °C by using a channel flow double electrode (CFDE) cell.[15] The CFDE cell can be operated as a closed system with the controlled oxygen concentration. From the hydrodynamic voltammograms under various laminar flow rates of the electrolyte solution, the kinetically controlled ORR activity at the planar working electrode can be evaluated. At the collecting electrode located at the downstream of the working electrode, H_2O_2 production rate, if any, can be quantified. In the present paper, we investigated temperature dependencies of the apparent ORR rate constant (k_{app}) activities and H_2O_2 production rate at Pt−Fe, Pt−Co, and Pt−Ni electrodes in 0.1 M $HClO_4$ solution at 20 to 90 °C by the CFDE method. We demonstrate the k_{app} at the alloy electrodes are larger than that at the Pt electrode by a factor of 4.0 ($Pt_{54}Fe_{46}$) to 2.4 ($Pt_{63}Ni_{37}$) in the temperature range from 20 to 50 °C and that H_2O_2 yield at the alloy electrodes is low, corresponding to 0.2−1.0% of the total ORR currents.

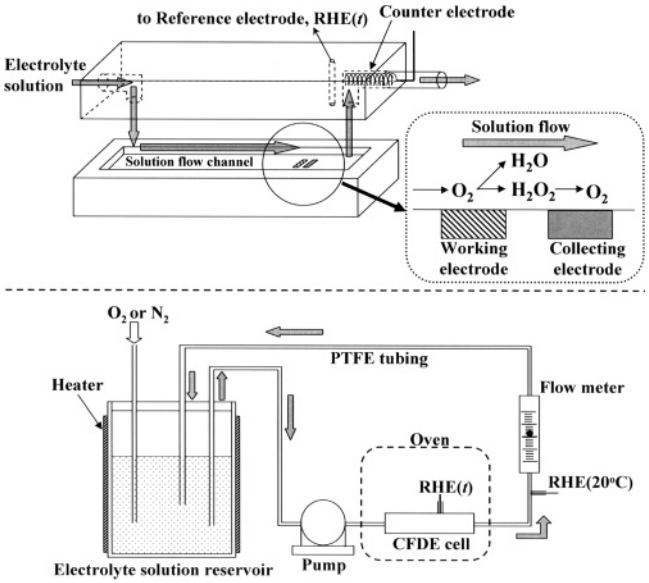

Figure 1. Schematic diagram of the channel flow double electrode (CFDE) cell (upper) and flow circuit of electrolyte solution (lower). The CFDE cell equipped with RHE(*t*), the electrolyte solution reservoir (made of PTFE), and the PTFE tubing were temperature controlled with a heater at 20 to 90 °C. RHE(20°C) was kept at 20 °C.

2. Experimental Section

Figure 1 shows the experimental setup of the channel flow double electrode cell and flow circuit of electrolyte solution. The CFDE cell was made of Kel-F blocks and a Teflon sheet,

* To whom correspondence should be addressed. Phone: +81-55-220-8620. Fax: +81-55-254-0371. E-mail: m-watanabe@yamanashi.ac.jp.
[†] Clean Energy Research Center, University of Yamanashi.
[‡] Interdisciplinary Graduate School of Medicine and Engineering, University of Yamanashi.

10.1021/jp046204+ CCC: $30.25
Published on Web 03/05/2005

resistant to hot acid electrolyte solution. As the working electrode, Pt alloy films (0.1 cm × 0.4 cm, geometric area A = 0.04 cm^2) were prepared on a gold substrate by Ar-sputtering (SH-33D, ULVAC Co Ltd.) a Pt target together with Fe, Co, or Ni targets at room temperature. The thickness of the films was controlled gravimetrically to about 0.1 μm. The resulting compositions determined by a fluorescent X-ray analysis (EDX-800, Shimadzu) were $Pt_{54}Fe_{46}$, $Pt_{68}Co_{32}$, and $Pt_{63}Ni_{37}$ in atomic ratio, which are almost the optimum compositions for the ORR obtained in our previous works[1,2] at room temperature. The crystallographic structures of these alloys were examined by grazing incidence (θ = 1°) X-ray diffraction (GIRD). GIRD patterns of these alloys indicated the formation of a solid solution with a face-centered cubic crystal structure. The Pt wire was used as a counter electrode. The reversible hydrogen electrode kept at the same temperature as that of the cell (t, °C) [denoted as RHE(t)] was used as the reference electrode. Another RHE [RHE(20°C)] was inserted in a portion of the exhaust tubing, cooled to room temperature, to check the change in the RHE(t) potential with changes of the cell operation temperature.[15,16]

The electrolyte solution of 0.1 M $HClO_4$ was prepared from reagent grade chemicals (Kanto Chemical Co.) and Milli-Q water (Milli-Pore Japan Co. Ltd.) and purified in advance with conventional pre-electrolysis methods.[17,18] The electrolyte solution was saturated with O_2 or N_2 gas bubbling them into the solution for at least 1 h prior to electrochemical measurements. Total pressure of the gas phase in the electrolyte solution reservoir was controlled with O_2 at 1.0 atm at 20 to 60 °C and 1.5 atm at 70 to 90 °C during ORR measurements. The oxygen concentration [O_2] and the diffusion coefficient D were calculated based on Henry's law and the Stokes−Einstein equation, respectively (see the Appendix in ref 15).

A bi-potentiostat (ALS 700B, BAS Inc.) was used for the CFDE measurement. Hydrodynamic voltammograms at the working electrode under a flow of O_2-saturated 0.1 M $HClO_4$ solution (mean flow rate = 10−50 cm s^{-1}) were recorded by scanning its potential from 0.3 to 1.0 V vs RHE(t) at 0.5 mV s^{-1}. To detect H_2O_2 emitted from the working electrode, the potential of the collecting electrode was set at 1.2 V vs RHE(t) where H_2O_2 was oxidized under a diffusion control condition. The collection efficiency (N) for the present CFDE system was experimentally determined to be 0.28 ± 0.01. During heating or cooling to a desired temperature, the potential of the working electrode was kept at 1.0 V vs RHE(t).

Electrochemical impedance measurements were carried out by using a computer-controlled frequency response analyzer (SI 1287 electrochemical interface and SI 1260 impedance/gain-phase analyzer, Solartron Analytical). Prior to the AC measurement, the potential of the working electrode was stepped to a desired potential and then held for 20 s, which is enough time to obtain a steady-state current in chronoamperometry. The AC modulation amplitude was 10 mV, and the frequency was swept from 10 kHz to 0.1 Hz.

3. Results and Discussion

3.1. Electrochemical Stabilization and Surface Roughness. As we reported, nonprecious metal elements in Pt−Fe, Pt−Co, and Pt−Ni alloys are leached out in an acidic solution, but a stable Pt skin of a few nanometers on the bulk alloys is formed on the alloy surfaces after the electrochemical stabilization treatment.[1,2,19] At room temperature by in situ scanning tunneling microscopy, we found that the dissolution of the surface alloy layer was followed by a rearrangement of the remaining Pt atoms on the surface.[20] Prior to ORR measurements, therefore, $Pt_{54}Fe_{46}$, $Pt_{68}Co_{32}$, and $Pt_{63}Ni_{37}$ electrodes were electrochemically stabilized by repetitive potential sweeps between 0.05 and 1.00 V vs RHE in N_2-purged 0.1 M $HClO_4$ solution at room temperature until a steady state cyclic voltammogram (CV) was obtained. Since the stabilized voltammograms resembled that of a polycrystalline platinum electrode, the electrochemically active surface area S was evaluated from an electric charge of hydrogen desorption wave ΔQ_H in each CV, supposing ΔQ_H° = 0.21 mC/cm^2 for a smooth polycrystalline Pt, as conventionally used.[17] The values of roughness factor R_f (ratio of S to geometric surface area A) are 9.2 ($Pt_{54}Fe_{46}$), 14 ($Pt_{68}Co_{32}$), and 7.3 ($Pt_{63}Ni_{37}$). Each ORR measurement was performed in O_2 saturated 0.1 M $HClO_4$ at 20 to 90 °C by recording the corresponding CV (the scan rate = 0.5 mV s^{-1}). The R_f of the electrode was checked after each ORR measurement in the same electrolyte solution by recording the corresponding CV. An influence of the ORR current on ΔQ_H° could be neglected by applying a rapid scan rate of 5 V s^{-1}. Figure 2 shows typical examples of CVs at the $Pt_{54}Fe_{46}$ electrode. The CVs obtained at 20 to 50 °C are hardly distinguished by the overlapping, but the current corresponding to ΔQ_H appreciably decreases with elevating temperature above 60 °C. As shown in Figure 3, the values of R_f at the $Pt_{54}Fe_{46}$ steeply decrease between 50 and 70 °C, so that the R_f at 90 °C is almost $^2/_3$ compared to that at 20 °C. More significant reduction in R_f is seen for $Pt_{68}Co_{32}$, while the reduction is relatively small for $Pt_{63}Ni_{37}$.

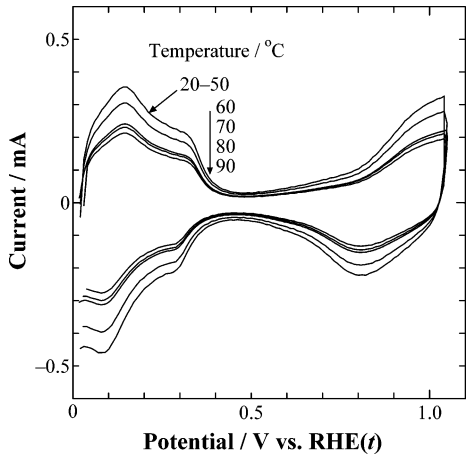

Figure 2. Cyclic voltammograms to determine the roughness factor R_f at $Pt_{54}Fe_{46}$ electrode in O_2 saturated 0.1 M $HClO_4$ solution at 20 to 90 °C. Potential scan rate = 5 V s^{-1}.

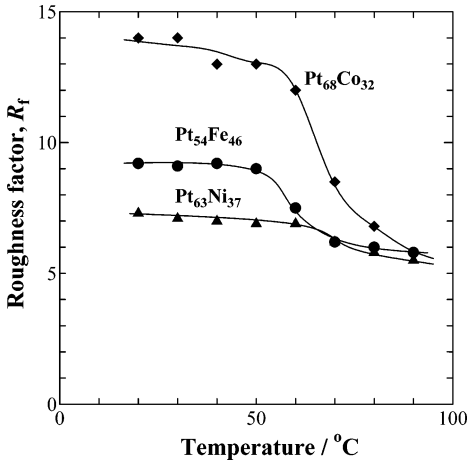

Figure 3. Changes in roughness factors R_f at (●) $Pt_{54}Fe_{46}$, (◆) $Pt_{68}Co_{32}$, and (▲) $Pt_{63}Ni_{37}$ electrodes with temperature.

3.2. Hydrodynamic Voltammetry for ORR. Figure 4 shows hydrodynamic voltammograms for the ORR at $Pt_{54}Fe_{46}$,

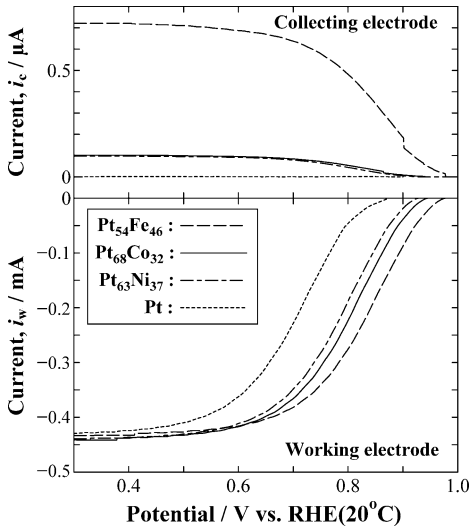

Figure 4. Hydrodynamic voltammograms for ORR in O_2 saturated 0.1 M $HClO_4$ solution at $Pt_{54}Fe_{46}$, $Pt_{68}Co_{32}$, $Pt_{63}Ni_{37}$, and Pt electrodes at 20 °C and simultaneously acquired currents (i_c) at Pt collecting electrodes. Potential scan rate = 0.5 mV s^{-1}. Potential of the collecting electrode = 1.2 V. Mean flow rate of electrolyte = 50 cm s^{-1}.

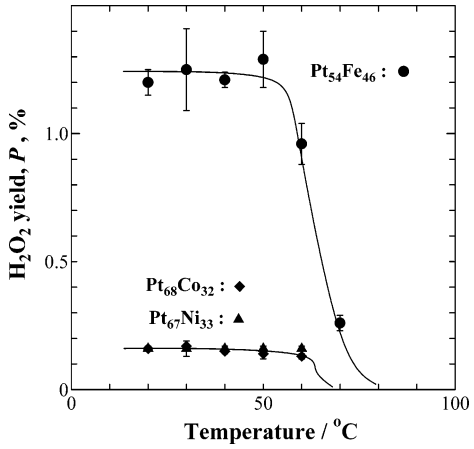

Figure 5. Temperature dependence of H_2O_2 yield at (●) $Pt_{54}Fe_{46}$, (◆) $Pt_{68}Co_{32}$, and (▲) $Pt_{63}Ni_{37}$ electrodes calculated by using eq 1. Potential of working electrode = 0.76 V vs RHE(t). Mean flow rate of electrolyte = 10−50 cm s^{-1}.

$Pt_{68}Co_{32}$, $Pt_{63}Ni_{37}$, and Pt working electrodes in O_2 saturated 0.1 M $HClO_4$ solution at 20 °C and simultaneously acquired currents at the Pt collecting electrodes. The ORR currents at the alloy electrodes commence to increase at about 0.95 V vs RHE(20°C), which is more positive than that at the pure Pt electrode by ca. 0.1 V, indicating enhanced catalytic activity of the Pt-skin layer formed on these alloys. Emission of H_2O_2 from the pure Pt working electrode is always below the detection limit (<ca. 5 nA) at the whole temperature range and the potential range of the working electrode. However, small oxidation currents of H_2O_2 at the collecting electrodes are observed for the alloy electrodes. The H_2O_2 yield (ratio of H_2O_2 production rate to that of the overall ORR), P (%), is calculated by

$$P = 2i_c/(Ni_w + i_c) \times 100\% \quad (1)$$

where i_w and i_c are the currents at the working and collecting electrodes, respectively. The values of P were found to be almost independent of the potential of each alloy working electrode between 0.3 and 0.8 V. As shown in Figure 5, the value of P is almost constant at 20−50 °C (1.2% at $Pt_{54}Fe_{46}$) or at 20−60 °C (0.16% at $Pt_{68}Co_{32}$ and $Pt_{63}Ni_{37}$). However, further elevation of temperature decreases H_2O_2 production below the detection limit (<0.05%). After the alloy electrodes experienced the high temperature in the acid electrolyte solution, the H_2O_2 production was never detected over the temperature range, even at low temperatures (20 to 60 °C).

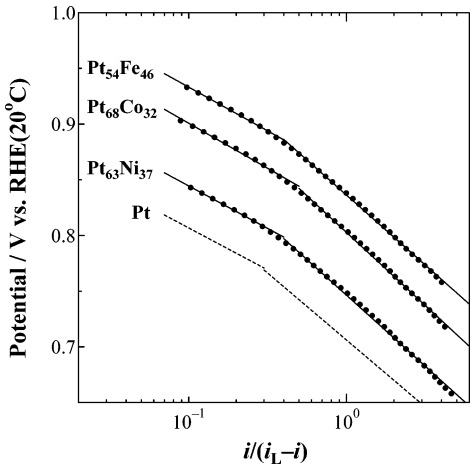

Figure 6. Tafel plots for the ORR at $Pt_{54}Fe_{46}$, $Pt_{68}Co_{32}$, $Pt_{63}Ni_{37}$, and Pt electrodes at 20 °C obtained from Figure 4.

Figure 6 shows Tafel plots [E vs $\log\{i/(i_L - i)\}$] for the ORR at the alloys in comparison with that of pure Pt at 20 °C, where i_L is the limiting current. The Tafel lines at alloys shift to more positive potential with the Tafel slope similar to that at the pure Pt electrode, i.e., ca. −120 mV/decade in the high current region and ca. −75 mV/decade in the low current region. This suggests that the rate determining step (rds) for the ORR is unchanged at both skin-layer Pt over such alloys and bulk Pt, despite the large differences of their electrocatalytic activities.

3.3. ORR Activity. The kinetically controlled current i_K at a given potential E is determined from the hydrodynamic voltammogram in the CFDE by using the following equation[21]

$$1/i = 1/i_K + 1/i_L = 1/i_K + 1/\{1.165 \times nF[O_2]w(U_m D^2 x_1^2/h)^{1/3}\} \quad (2)$$

where n is the number of electrons transferred, F is the Faraday constant, $[O_2]$ is the O_2 concentration in the bulk of the electrolyte solution, w is the width of the working electrode, U_m is the mean flow rate of the electrolyte solution, D is the diffusion coefficient of O_2, x_1 is the length of the working electrode in the electrolyte flow direction, and h is the half channel height (or the half thickness of the electrolyte flow over the electrodes). Figure 7 shows plots of i^{-1} vs $U_m^{-1/3}$ obtained at 0.760 V vs RHE at 30 °C (−0.525 V vs $E°$). Linear relationships are seen at all the electrodes. The number of electrons calculated from the slopes with eq 2 was found to be 4.0 ± 0.2, which is consistent with the results described above. By extrapolating $U_m^{-1/3}$ to 0 (infinite flow rate), the value of i_K was determined. However, the value of i_K is not a suitable measure for the ORR activity because the i_K depends on the $[O_2]$ in the electrolyte solution, which decreases with elevating the operating temperature. Since the contribution of two-electron reduction to produce H_2O_2 (to the overall ORR) was very low (see Figure 5), we can calculate an apparent rate constant k_{app} at a constant overpotential at 20 to 90 °C, in the same manner as in our previous work for pure Pt,[15]

$$i_K/(4FS) = -k_{app}[H^+][O_2] \quad (3)$$

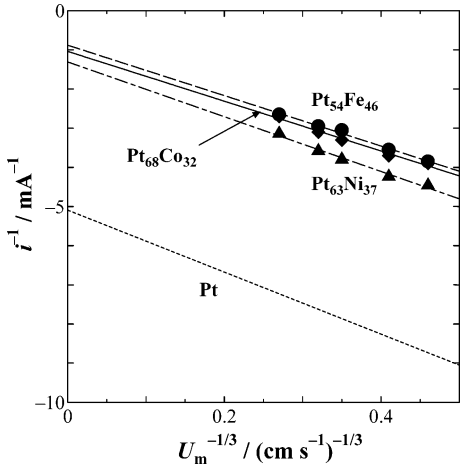

Figure 7. i^{-1} vs $U_m^{-1/3}$ plots obtained from hydrodynamic voltammograms for ORR at (●) $Pt_{54}Fe_{46}$, (◆) $Pt_{68}Co_{32}$, (▲) $Pt_{63}Ni_{37}$, and (···) Pt electrodes at 20 °C and at −0.525 V vs $E°$.

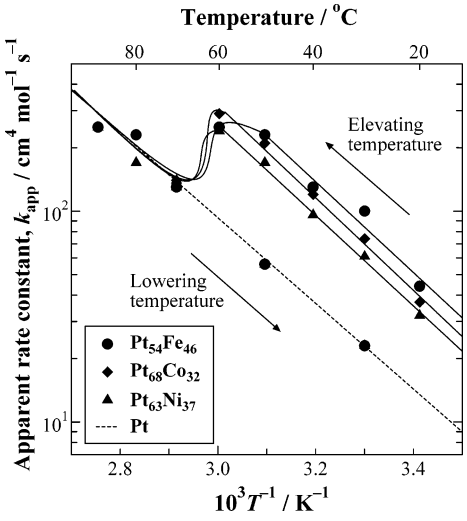

Figure 8. Arrhenius plots of apparent rate constant k_{app} for the ORR at (●) $Pt_{54}Fe_{46}$, (◆) $Pt_{68}Co_{32}$, (▲) $Pt_{63}Ni_{37}$, and (···) Pt electrodes at −0.525 V vs $E°$.

where $[H^+]$ is the bulk concentration of H^+ (0.1 M) and S is an electrochemically active area ($R_f \times A$) at each temperature. Figure 8 shows Arrhenius plots of k_{app} on the alloy electrodes at −0.525 V vs $E°$ in comparison with that of pure Pt electrode. Since both $E°$ and E[RHE(t)] shift to less positive values with elevating temperature, the corrected potential E is applied so as to keep a constant overpotential at each temperature.[15] In the low-temperature region (20−50 °C for $Pt_{54}Fe_{46}$, 20−60 °C for $Pt_{68}Co_{32}$ and $Pt_{63}Ni_{37}$), linear relationships between log k_{app} and $1/T$ are observed at all the electrodes, corresponding to the following Arrhenius equation.

$$k_{app} = Z \exp(-\epsilon_a/RT) \tag{4}$$

An apparent activation energy ϵ_a on each alloy was found to be 41 kJ mol^{-1}, which is comparable to that on the pure Pt electrode of 38 kJ mol^{-1}. The value of k_{app} on the alloys is larger than that on the Pt electrode by a factor of 4.0 ($Pt_{54}Fe_{46}$), 3.1 ($Pt_{68}Co_{32}$), and 2.4 ($Pt_{63}Ni_{37}$), respectively. However, the k_{app} values on the alloys rather decrease with elevating temperature above 60 °C, and settle at almost the same value as the Pt electrode. The degraded ORR activity after heating at the high temperature in the solution was never recovered even in the low-temperature region and exhibited almost the same k_{app} as that of the pure Pt electrode. It is noted that the critical temperature of ca. 60 °C for losing the high ORR activity corresponds well with that of sharp reduction in R_f (Figure 3) and that of losing H_2O_2 production activity (Figure 5). This indicates that the Pt skin layer formed on the alloy electrodes by the pretreatment mentioned above can stand at temperatures <60 °C but increases the thickness beyond this temperature, resulting in the property of bulky pure Pt, due to the enhanced dissolution of nonprecious metals from the underlying alloys.

3.4. Mechanism of Enhancement of ORR Activities at Pt Alloy Electrodes. Then, we discuss the mechanism of enhanced specific ORR activities (k_{app}) at the Pt skin layer on the alloys. The Tafel slope of −120 mV/decade at the high current density region indicates that the enhancement in the ORR activities at Pt skin layers over these alloys is dominantly brought about by promoting the same rds of the first one-electron-transfer step as that of pure Pt.[1,2] Considering the first-order dependence of the ORR rate on $[O_2]$[15] and pH,[22] the rds can be written as follows.

$$x\mathrm{Pt} + \mathrm{O_2} + \mathrm{H^+} + \mathrm{e^-} \rightarrow \mathrm{Pt}_x\mathrm{-\dot{O}_2-H} \tag{5}$$

This reaction may consist of the following elementary steps:

$$\mathrm{Pt}_x\mathrm{-}y\mathrm{A_{ad}} + \mathrm{O_2} \rightleftarrows \mathrm{Pt}_x\mathrm{-O_2} + y\mathrm{A_{ad}} \quad (\mathrm{A_{ad}} = \mathrm{H_2O} \text{ or adsorbed anions}) \tag{6}$$

$$\mathrm{Pt}_x\mathrm{-O_2} + \mathrm{H^+(H_2O)}_z \rightleftarrows [\mathrm{Pt}_x\mathrm{-O_2\cdots H^+\cdots (H_2O)}_z]^* \tag{7}$$

$$[\mathrm{Pt}_x\mathrm{-O_2\cdots H^+\cdots (H_2O)}_z]^* + \mathrm{e^-} \rightarrow \mathrm{Pt}_x\mathrm{-\dot{O}_2-H} + z(\mathrm{H_2O}) \tag{8}$$

where the asterisk denotes the activated complex. Because the activation energy ϵ_a on both alloys and pure Pt is the same, the high ORR activities at the alloys are ascribed to a large preexponential factor Z in the rate constant of eq 4. As reported previously,[1,2] the electronic state at the Pt skin is strongly modified by underlying alloy. This may increase the coverage of adsorbed oxygen, e.g., in the reaction step 6. To clarify an influence of the change in the oxygen coverage on the ORR mechanism, we focus on the H_2O_2 production during the ORR at all the alloy electrodes operated at low temperatures in the next section.

3.5. Mechanism of H_2O_2 Production at the Alloys. Recently, Itagaki et al.[23,24] proposed a theoretical model for the electrochemical impedance spectra corresponding to various ORR paths in an alkaline solution using a CFDE cell at room temperature. According to their criteria, the second capacitive semicircle or an inductive loop in the low-frequency range appears in the complex plane plot of the electrochemical impedance, when the reaction proceeds via an adsorbed intermediate such as H_2O_2. Figure 9 shows complex plane plots of the electrochemical impedance obtained on the $Pt_{54}Fe_{46}$ working electrode at 30 °C in the high potential region (0.87 V vs RHE) and in the limiting current region (0.40 V vs RHE). The impedance plots show only a capacitive semicircle and the second capacitive semicircle as well as the inductive one are not observed. This behavior is just the same as that of pure Pt,[15] suggesting that the adsorbed H_2O_2 is not a stable intermediate even on the alloy.

It has been reported that H_2O_2 can be generated even at the pure Pt electrode in acidic solutions in the presence of some adsorbates such as chloride,[25,26] bromide,[27] or under-potentially deposited (UPD) hydrogen atom[8] (at E < 0.3 V). Taking such an effect of adsorbates on the H_2O_2 production together with

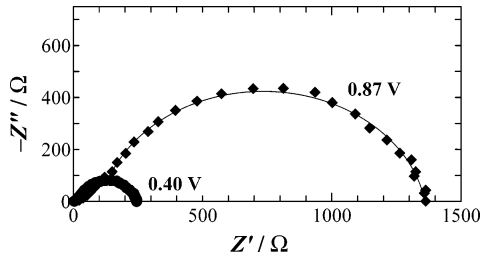

Figure 9. Complex plane plots of the electrochemical impedance for the ORR at the $Pt_{54}Fe_{46}$ working electrode in O_2 saturated 0.1 M $HClO_4$ solution at 30 °C. DC potentials of the electrode were set at (●) 0.40 and (◆) 0.87 V vs RHE. The AC modulation amplitude to the electrode was 10 mV. $U_m = 50$ cm s^{-1}.

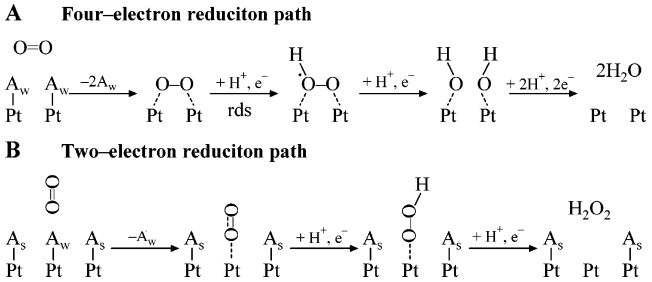

Figure 10. Reaction schemes for (A) four- and (B) two-electron reduction paths. A_s and A_w stand for the weak and strong adsorbates, respectively.

our results described above into consideration, we propose reaction paths for four- and two-electron ORRs, respectively, as illustrated in Figure 10. An oxygen molecule occupying two Pt sites by side-on adsorption is assumed to be reduced to form water (four-electron path in Figure 10A). On the other hand, end-on O_2 adsorption occupying only one Pt site can lead to H_2O_2 production, if H_2O_2 desorbs into the solution after two-electron reduction (Figure 10B). The former case may be dominant for the Pt surface without any impurity adsorbates or only with weakly bonding adsorbates (such as water or perchlorate anion). When neighboring Pt sites are blocked by strongly bonding adsorbates (such as halides or UPD hydrogen atoms), the possibility of the end-on adsorption should increase. Recent theoretical calculations for the four-electron ORR on Pt support our hypothesis[28,29] Electronic modification of the Pt skin layer, i.e., larger 5d-electron vacancy than the pure Pt, probably enhances not only the overall ORR rate but also the possibility of end-on type O_2 adsorption due to increase in the coverage (by a factor of 2 to 4 corresponding to the increased Z values mentioned above) and the bond strength. This must result in such an increased H_2O_2 production shown in Figure 5. Thus, the largest amount of H_2O_2 is produced at the $Pt_{54}Fe_{46}$ with the highest ORR activity among the alloys we investigated. We can reject the possibility of the H_2O_2 intermediate in an indirect four-electron reduction at the alloys, as often discussed based on Wroblowa's reaction scheme,[30] because, at the $Pt_{54}Fe_{46}$ electrode, reduction steps following to the rds of the first one-electron transfer are so facile that a stable adsorbed intermediate could not be detected.

3.6. Irreversible Change in the ORR Activity by Corrosion. The ORR activity and H_2O_2 production rate at the Pt skin layer on the alloys drastically decrease after operated at a temperature between 50 and 70 °C in the electrolyte solution. Such a "deactivated" electrode exhibits just the same electrochemical properties as the pure Pt, not only in the high-temperature region but also in the low-temperature region. This is certainly ascribed to a dealloying of the nonprecious metal component in a hot acid solution, resulting in a thick Pt layer, the electronic state of which is no longer affected by the underlying alloy. It is noted, however, that the surface roughness of the alloys decreases sharply at the same temperature region as shown in Figure 3. This is due to an increased migration rate of surface Pt atoms at elevated temperature.

The trend of the ORR activity in the order Pt < Pt−Ni < Pt−Co < Pt−Fe is the same as that at the alloy rotating disk electrodes of similar compositions, examined only at room temperature.[1] However, the magnitude of the enhancement in the ORR activity obtained in the present alloys is smaller than those obtained in our previous work (10−20 times higher activities than the pure Pt). At the present stage, we cannot understand why such a big difference in the enhancement of the ORR activity occurred. However, the present results reveal that Pt−Fe, Pt−Co, or Pt−Ni alloys are effective ORR catalysts for PEFCs operated lower than 50 °C.

4. Conclusions

The ORR activities and the H_2O_2 formations at $Pt_{54}Fe_{46}$, $Pt_{68}Co_{32}$, and $Pt_{63}Ni_{37}$ electrodes in 0.1 M $HClO_4$ solution at 20 to 90 °C were quantitatively investigated with the CFDE method. It was found that the ORR rates at these alloy electrodes are 2.4−4.0-fold larger than that at the pure Pt electrode between 20 and 60 °C and that the ORR activity increases in the order Pt < $Pt_{63}Ni_{37}$ < $Pt_{68}Co_{32}$ < $Pt_{54}Fe_{46}$. The apparent activation energy (41 kJ mol^{-1} at −0.525 V vs $E°$) and the rds for the ORR at the alloy electrodes are the same as those of the pure Pt electrode. A small amount of H_2O_2 formation is observed at all the alloy electrodes [ca. 1.0% at $Pt_{54}Fe_{46}$ and ca. 0.16% at $Pt_{68}Co_{32}$ and $Pt_{63}Ni_{37}$ between 20 and 60 °C]. The enhanced ORR activities of the alloy electrodes are ascribed to increase in the preexponential factor in the Arrhenius equation, maybe relating to an increased O_2 coverage. The alloys lost high ORR activities and the H_2O_2 production was down to the levels of the pure Pt electrode at temperatures higher than 60 °C because of the dealloying.

Acknowledgment. This work was partly supported by CREST of Japan Science and Technology Agency and also was supported by the fund for "Leading Project" of Ministry of Education, Science, Culture, Sports and Technology of Japan.

References and Notes

(1) Toda, T.; Igarashi, H.; Uchida, H.; Watanabe, M. *J. Electrochem. Soc.* **1999**, *146*, 3750.
(2) Toda, T.; Igarashi, H.; Watanabe, M. *J. Electroanal. Chem.* **1999**, *460*, 258.
(3) Toda, T.; Honma, I. *Trans. Mater. Res. Soc. Jpn.* **2003**, *28*, 215.
(4) Mukerjee, S.; Srinivasan, S.; Soriaga, M. P.; McBreen, J. *J. Electrochem. Soc.* **1995**, *142*, 1409.
(5) Mukerjee, S.; Srinivasan, S. *J. Electroanal. Chem.* **1993**, *357*, 201.
(6) Min, M.; Cho, J.; Cho, K.; Kim, H. *Electrochim. Acta* **2000**, *45*, 4211.
(7) Neergat, N.; Shukla, A. K.; Gandhi, K. S. *J. Appl. Electrochem.* **2001**, *31*, 373.
(8) Stamenkovic, V.; Schmidt, T. J.; Markovic, N. M.; Ross, P. N., Jr. *J. Phys. Chem. B* **2002**, *106*, 11970.
(9) Stamenkovic, V.; Schmidt, T. J.; Ross, P. N.; Markovic, N. M. *J. Electroanal. Chem.* **2003**, *554−555*, 191.
(10) Drillet, J.-F.; Ee, A.; Friedemann, J.; Kötz, R.; Schnyder, B.; Schmidt, V. M. *Electrochim. Acta* **2002**, *47*, 1983.
(11) Yang, H.; Vogel, W.; Lamy, C.; Alonso-Vante, N. *J. Phys. Chem. B* **2004**, *108*, 11024.
(12) Paffett, M. T.; Berry, J. G.; Gottesfeld, S. *J. Electrochem. Soc.* **1988**, *135*, 1431.
(13) Thamizhmani, G.; Capuano, G. A. *J. Electrochem. Soc.* **1994**, *141*, 968.
(14) Antolini, E.; Passos, R. R.; Ticianelli, E. A. *Electrochim. Acta* **2002**, *48*, 263.

(15) Wakabayashi, N.; Takeichi, M.; Itagaki, M.; Uchida, H.; Watanabe, M. *J. Electroanal. Chem.* **2005**, *574*, 339.
(16) Wakabayashi, N.; Uchida, H.; Takeuchi, K.; Watanabe, M. *Electrochem. Solid-State Lett.* **2002**, *5*, E62.
(17) Watanabe, M.; Motoo, S. *J. Electroanal. Chem.* **1975**, *60*, 259.
(18) Uchida, H.; Ikeda, N.; Watanabe, M. *J. Electroanal. Chem.* **1997**, *424*, 5.
(19) Uchida, H.; Ozuka, H.; Watanabe, M. *Electrochim. Acta* **2002**, *47*, 3629.
(20) Wang, L.-J.; Moriyama, T.; Ito, M.; Uchida, H.; Watanabe, M. *Chem. Commun.* **2002**, 58.
(21) Levich, V. G. In *Physicochemical Hydrodynamics*; Prentice Hall: Englewood Cliffs, NJ, 1962; p 112.
(22) Sepa, D. B.; Vojnovic, M. V.; Damjanovic, A. *Electrochim. Acta* **1981**, *26*, 781.
(23) Itagaki, M.; Hasegawa, H.; Watanabe, K.; Hachiya, T. *J. Electroanal. Chem.* **2003**, *557*, 59.
(24) Itagaki, M.; Hasegawa, H.; Watanabe, K.; Hachiya, T. *Electrochemistry* **2003**, *71*, 536.
(25) Schmidt, T. D.; Paulus, U. A.; Gasteiger, H. A.; Behm, R. J. *J. Electroanal. Chem.* **2001**, *508*, 41.
(26) Stamenkovic, V.; Markovic, M. N.; Ross, P. N., Jr. *J. Electroanal. Chem.* **2001**, *500*, 44.
(27) Markovic, M. N.; Gasteiger, H. A.; Grgur, B. N.; Ross, P. N. *J. Electroanal. Chem.* **1999**, *467*, 157.
(28) Sidik, R. A.; Anderson, A. B. *J. Electroanal. Chem.* **2002**, *528*, 69.
(29) Anderson, A. B.; Albu, T. *J. Electrochem. Soc.* **2000**, *147*, 4229.
(30) Wroblowa, H. S.; Pan, Y. C.; Razumney, G. *J. Electroanal. Chem.* **1976**, *69*, 195.